MOSIC: Model-Agnostic Optimal Subgroup Identification with Multi-Constraint for Improved Reliability

Wenxin Chen¹, Weishen Pan¹, Kyra Gan¹, Fei Wang¹,

 $^{1} Cornell\ University\\ wc 645 @cornell.edu,\ wep 4001 @med.cornell.edu,\ kyragan @cornell.edu,\ few 2001 @med.cornell.edu$

Abstract

Current subgroup identification methods typically follows a two-step approach: first estimate conditional average treatment effects (CATEs) and then apply thresholding or rulebased procedures to define subgroups. While intuitive, this decoupled approach fails to incorporate key constraints essential for real-world clinical decision-making—such as subgroup size and propensity overlap. These constraints operate on fundamentally different axes than CATE estimation and are not naturally accommodated within existing frameworks, thereby limiting the practical applicability of these methods. We propose a unified optimization framework that directly solves the *primal* constrained optimization problem to identify optimal subgroups. Our key innovation is a reformulation of the constrained primal problem as an unconstrained differentiable min-max objective, solved via a gradient descentascent algorithm. We theoretically establish that our solution converges to a feasible and locally optimal solution. Unlike threshold-based CATE methods that apply constraints as post-hoc filters, our approach enforces them directly during optimization. The framework is model-agnostic, compatible with a wide range of CATE estimators, and extensible to additional constraints like cost limits or fairness criteria. Extensive experiments on synthetic and real-world datasets demonstrate its effectiveness in identifying high-benefit subgroups while maintaining better satisfaction of constraints.

1 Introduction

In precision medicine, a fundamental challenge in observational studies is identifying patient subgroups that benefit most from specific treatments, where heterogeneous effects must be estimated from non-randomized data (Kosorok and Laber 2019; Kravitz, Duan, and Braslow 2004). Most existing methods adopt a two-step paradigm: they first estimate CATEs using machine learning methods (Athey and Imbens 2016; Shalit, Johansson, and Sontag 2017; Shi, Blei, and Veitch 2019), then deriving subgroups through either thresholding (VanderWeele et al. 2019; Lipkovich et al. 2024) or simplified rule-based models (Cai et al. 2022).

However, this two-stage approach falls short when applied to real-world settings, where subgroup identification must account for diverse and interacting constraints. Clinical deployment often requires satisfying statistical conditions

Copyright © 2026, Association for the Advancement of Artificial Intelligence (www.aaai.org). All rights reserved.

like minimum subgroup size and overlap (VanderWeele et al. 2019; Crump et al. 2009), as well as operational and ethical considerations such as budget limits, safety thresholds, and fairness criteria. Existing methods typically treat these constraints as post-hoc filters rather than integrating them into the optimization process. As a result, they *struggle to jointly satisfy multiple constraints*, leading to instability and poor performance. These challenges highlight a deeper disconnect between the continuous nature of CATE estimates and the discrete, constraint-driven structure of clinically actionable subgroup identification. This motivates the need for new frameworks that can incorporate and optimize over multiple real-world constraints in a unified and principled way.

We propose MOSIC (Model-agnostic Optimal Subgroup Identification with multi-Constraints), a *novel optimization* framework that identifies subgroups with maximal CATE while satisfying group size and overlap constraints—with flexibility to incorporate additional constraints. Our approach addresses the key challenge of nonconvex/nonconcave optimization, and our contributions are threefold:

- Problem Reformulation for Stable Solutions: We develop a stable optimization procedure that: (1) formulates the task as a constrained problem (Section 3.1), (2) absorbs constraints into the objective via a reformulation (Section 3.2), and (3) solves it using a gradient descent-ascent (Section 4.1). To improve stability, we modify the objective (Section 4.2) and establish that the resulting solution is locally optimal and feasible.
- Flexibility: MOSIC maintains unique flexibility across three dimensions: (1) supporting multiple subgroup model architectures (e.g., multilayer perceptrons, decision trees) for different interpretability-performance tradeoffs, (2) compatibility with various ATE estimators, and (3) extensibility to diverse clinical constraints beyond our focus on size and overlap requirements.
- Comprehensive Evaluation: We extensively evaluate our framework on both synthetic and real-world data, demonstrating its effectiveness in optimal subgroup identification under multiple constraints (Section 5). Our implementation is publicly available at https://anonymous. 4open.science/r/MOSIC3-8F13.

2 Related Work

We review treatment effect estimation, overlap handling, subgroup identification, and constrained optimization methods, highlighting that multi-constraints subgroup identification remains under-explored.

Treatment Effect Estimation MOSIC accommodates various average treatment effect (ATE) estimators. Traditional methods like IPTW and meta-learners (e.g., S-, T-, X-learners, Künzel et al. 2019) rely on either the treatment or outcome model, making them sensitive to misspecification. In contrast, doubly robust estimators such as AIPTW (Robins, Rotnitzky, and Zhao 1995), targeted maximum likelihood estimation (TMLE) (Van Der Laan and Rubin 2006), and DML (Chernozhukov et al. 2018) require only one model (treatment or outcome) to be correctly specified. In this paper, we adopt AIPTW for illustration.

While ATE captures population-level effects, CATE estimation enables subgroup-specific recommendations. Modern methods include 1) tree-based methods like Causal Tree (CT) (Athey and Imbens 2016) and Causal Forest (CF) (Wager and Athey 2018), and 2) neural network-based approaches, such as TARNet and CFR (Shalit, Johansson, and Sontag 2017), Dragonnet (Shi, Blei, and Veitch 2019), and BCAUSS (Tesei et al. 2023). Notably, Dragonnet includes a TMLE-inspired regularization term for enhanced finite-sample stability. In this work, to construct our AIPTW estimator, we use Dragonnet to estimate the potential outcome models and use LR to estimate the propensity score model.

Dealing with Limited Overlap Limited sample overlap can bias treatment effect estimates or inflate variance (Crump et al. 2009). Common solutions include truncating propensity scores (Gruber et al. 2022; Cole and Hernán 2008) and excluding low-overlap units (Crump et al. 2009; Schweisthal et al. 2024; Kallus 2020). To ensure reliable ATE estimation on the identified subgroup, we incorporate a set of constraints to avoid regions with limited overlap.

Optimal Subgroup Identification Existing approaches fall into three concise categories: (i) *baseline methods* without interpretability or constraints, (ii) methods emphasizing *interpretability*, and (iii) methods designed to incorporate domain-specific *constraints*.

Common subgroup identification methods either: (1) rank patients by estimated CATE values (Cai et al. 2011; Vander-Weele et al. 2019) (benchmarked this approach employing CT, CF, and Dragonnet as CATE estimators in Section 5), or (2) optimize individual treatment rules using methods like Outcome-Weighted Learning (OWL) (Zhao et al. 2012; Liu et al. 2018), which frames treatment as a weighted classification problem. While providing useful baselines, these methods do not readily accommodate additional constraints, a limitation our approach addresses.

For *interpretability*, *Decision Tree* (DT)-based methods are widely used (Foster, Taylor, and Ruberg 2011; Lipkovich et al. 2011; Dusseldorp, Doove, and Mechelen 2016; Huang et al. 2017; Athey and Wager 2021). A representative example is Virtual Twins (VT) (Foster, Taylor, and Ruberg 2011).

It first estimates CATE and then applies a DT for interpretable subgroup identification. Beyond trees, rule learning approaches have been adopted (Wang and Rudin 2021; Zhou et al. 2024). However, these methods rely on combinatorial searches and do not scale. Our method can instead leverage DTs as the backbone model, achieving the same level of interpretability while remaining scalable. We compare its performance against other DT-based methods in Section 5.4.

While single *constraints* like minimum group size can be applied post hoc to CATE estimates (VanderWeele et al. 2019), multi-constraint problems often require directly optimization to yield better outcomes. CAPITAL (Cai et al. 2022) is the most closely related approach to ours: it maximize subgroup size under an average CATE threshold and allow extension to a single constraint using Lagrangian relaxation. However, it struggles with multiple constraints due to instability and lack of feasibility guarantees. In Section 5, we compare our approach with VT, OWL, and CAPITAL.

Constrained Optimization Constrained optimization algorithms vary by problem convexity. For convex objective and constraints, classical methods such as Projected Gradient Descent (PGD), Frank-Wolfe (FW), Interior Point Methods (IPM), and Lagrangian-based methods (e.g., Alternating Direction Method of Multipliers, ADMM, Boyd et al. 2011) are effective. For non-convex objectives with convex feasible regions, global optimality is NP-hard and convergence guarantees weaken (Lacoste-Julien 2016; Wang, Yin, and Zeng 2019). Our setting—non-convex objective with nonconvex constraints—poses greater challenges: PGD struggles with complex prediction, IPM scales poorly with constraint count, FW assumes convexity, and Lagrangian methods often lack stability and feasibility guarantees. ADMM fails here due to the non-separable objective. While ADMM variants exist for structured problems (Gao, Goldfarb, and Curtis 2020), none apply to our setting. In contrast, our method guarantees both constraint feasibility and local optimality, critical for real-world deployment.

3 Problem Settings

Let $X \in \mathcal{X} \subseteq \mathbb{R}^d$ denote baseline covariates, $A \in \mathcal{A} = \{0,1\}$ the treatment (0: control, 1: treatment), and $Y \in \mathcal{Y}$ the outcome, which may be binary $(\mathcal{Y} = 0,1)$ or continuous $(\mathcal{Y} \subseteq \mathbb{R})$. The observational dataset consists of n samples $(\boldsymbol{x}i,a_i,y_i)_{i=1}^n$. Let Y(0) and Y(1) denote the potential outcomes under control and treatment. The propensity score is denoted as $e(\boldsymbol{x}) = P(A = 1|\boldsymbol{X} = \boldsymbol{x})$, and potential outcomes as $\mu_a(\boldsymbol{x}) = \mathbb{E}[Y|\boldsymbol{X} = \boldsymbol{x}, A = a]$.

We adopt standard causal inference assumptions: 1) Stable Unit Treatment Value Assumption (SUTVA): $Y = A \cdot Y(1) + (1 - A) \cdot Y(0)$; 2) Unconfoundedness: $\{Y(0), Y(1)\} \perp A | \mathbf{X};$ 3) Overlap: $0 < e(\mathbf{x}) < 1, \forall \mathbf{x} \in \mathcal{X}.$

3.1 Reliable Subgroup Identification Framework

In this framework, our goal is to identify a patient subgroup with the largest ATE while ensuring reliability. We achieve this by learning a subgroup identification model $\tilde{S}: \mathbb{R}^d \mapsto \{0,1\}$, which assigns a patient with covariates $\boldsymbol{X} = \boldsymbol{x}$ to

the subgroup $(\tilde{S}(\boldsymbol{x})=1)$ or excludes them $(\tilde{S}(\boldsymbol{x})=0)$. We define the subgroup's ATE as:

$$\mathbb{E}[Y(1) - Y(0)|\tilde{S}(\boldsymbol{X}) = 1] =$$

$$\mathbb{E}\left[\mathbb{E}[Y|A = 1, \boldsymbol{X}] - \mathbb{E}[Y|A = 0, \boldsymbol{X}]|\tilde{S}(\boldsymbol{X}) = 1\right], \quad (1)$$

following from the assumptions of SUTVA and unconfoundedness, and the inner expectations in Equation (1) represent the pseudo-outcomes on each sample.

Let $\hat{\phi}(\boldsymbol{x}_i, a_i, y_i)$ denote the estimated pseudo-outcomes for each sample, a general estimator for the subgroup's ATE, can then be written as:

$$\frac{\sum_{i=1}^{n} \mathbb{1}(\tilde{S}(X) = 1)\hat{\phi}(x_i, a_i, y_i)}{\sum_{i=1}^{n} \mathbb{1}(\tilde{S}(X) = 1)},$$

where $\mathbb{1}(\cdot)$ is the indicator function.

In addition to maximizing the treatment effect on the identified subgroup, we introduce the following constraints:

- Minimum subgroup size requirement. A sufficiently large subgroup is essential for ensuring reliable treatment effect estimation and practical applicability. For instance, maintaining adequate statistical power is crucial for robust analysis, and in drug repurposing, having enough responders makes a treatment economically viable.
- Each sample in the identified subgroup adheres to the overlap assumption. Similar to excluding samples with extreme propensity scores (Crump et al. 2009), we impose that *each sample* in the selected subgroup has a propensity score bounded away from 0 and 1.

The above task can be formally stated as follows:

$$\begin{aligned} & \min_{\tilde{S}} \ -\frac{\sum_{i=1}^{n} \mathbb{1}(\tilde{S}(\boldsymbol{X}) = 1) \hat{\phi}(\boldsymbol{x}_{i}, a_{i}, y_{i})}{\sum_{i=1}^{n} \mathbb{1}(\tilde{S}(\boldsymbol{X}) = 1)} & \textbf{(Problem I)} \\ & \text{s.t.} \quad \mathbb{E}\left[\tilde{S}(\boldsymbol{X})\right] \geq c \\ & \alpha \leq e(\boldsymbol{x}) \leq 1 - \alpha, \forall \boldsymbol{x} : \tilde{S}(\boldsymbol{x}) = 1, \end{aligned} \tag{2}$$

where $c \in (0,1)$ is the desired size of the subgroup, and $\alpha \in [0,0.5)$ is the threshold controlling the overlap constraint. While we focus on the subgroup size and overlap constraints here, our method naturally accommodates more general **linear and ratio-form constraints**, which we formally introduce in Lemma 2 and Remark 2 (Section 4.2).

3.2 Relaxing the Combinatorial Formulation

Since the **Problem I** is combinatorial and difficult to optimize, we relax the subgroup identification to a probabilistic assignment. This relaxation is implemented using a parametric surrogate model $S: \mathbb{R}^d \mapsto (0,1)$ with parameters $\pmb{\theta}$. The ATE on the identified subgroup can be expressed as

$$f(\boldsymbol{\theta}) = \frac{\sum_{i=1}^{n} S(\boldsymbol{x}_i; \boldsymbol{\theta}) \hat{\phi}(\boldsymbol{x}_i, a_i, y_i)}{\sum_{i=1}^{n} S(\boldsymbol{x}_i; \boldsymbol{\theta})}.$$
 (3)

Let $\hat{e}(\boldsymbol{x}_i)$, $\hat{\mu}_a(\boldsymbol{x}_i)$ denote the estimated $e(\boldsymbol{x}_i)$ and $\mu_a(\boldsymbol{x}_i)$. We then adopt the AIPTW estimator, which can be expressed as functions of $\hat{e}(\boldsymbol{x}_i)$ and $\hat{\mu}_a(\boldsymbol{x}_i)$:

$$\hat{\phi}_{\text{aiptw}}(\boldsymbol{x}_i, a_i, y_i) = \hat{\mu}_1(\boldsymbol{x}_i) - \hat{\mu}_0(\boldsymbol{x}_i) + \frac{a_i}{\hat{e}(\boldsymbol{x}_i)} (y_i - \hat{\mu}_1(\boldsymbol{x}_i))$$
$$-\frac{1 - a_i}{1 - \hat{e}(\boldsymbol{x}_i)} (y_i - \hat{\mu}_0(\boldsymbol{x}_i)). \tag{4}$$

While this study focus on AIPTW, $\hat{\phi}(x_i, a_i, y_i)$ can be derived using other ATE estimators, making this formulation flexible. More details are illustrated in Appendix C.1.

Due to the relaxation of subgroup identification into a probabilistic assignment, Constraint (2), originally designed for discrete subgroup selection, must be adapted. To achieve this, we introduce $h(\boldsymbol{x}_i, \alpha)$, a surrogate function that reformulates the overlap constraint from **Problem I**:

$$h(\boldsymbol{x}_i, \alpha) = 1 - \frac{\hat{e}(\boldsymbol{x}_i)(1 - \hat{e}(\boldsymbol{x}_i))}{\alpha(1 - \alpha)}.$$
 (5)

The following result, Lemma 1 (proof in Appendix B.1), establishes that Constraint (2) in **Problem I** can be replaced by a constraint on $h(x_i, \alpha)$:

Lemma 1. $S(\mathbf{x}_i; \boldsymbol{\theta}) h(\mathbf{x}_i, \alpha) \leq 0$ if and only if $\alpha \leq \hat{e}(\mathbf{x}_i) \leq 1 - \alpha$.

With Lemma 1, our optimization can be reformulated as:

$$\min_{\boldsymbol{\theta}} \quad -f(\boldsymbol{\theta}) \tag{Problem II}$$

s.t.
$$\frac{1}{n} \sum_{i=1}^{n} S(\boldsymbol{x}_i; \boldsymbol{\theta}) \ge c$$
 (6)

$$S(\boldsymbol{x}_i; \boldsymbol{\theta}) h(\boldsymbol{x}_i, \alpha) \le 0, \forall i.$$
 (7)

Solving **Problem II** remains a significant challenge. As shown in Equation (3), the parametric model $S(\boldsymbol{x_i};\boldsymbol{\theta})$ appears in both the numerator and denominator, making the objective function $f(\boldsymbol{\theta})$ neither convex nor concave, even for simple models like logistic regression. This nonconvexity also extends to the feasible set, rendering standard convex optimization methods, such as ADMM and FW unsuitable. Although it could, in principle, be solved using Lagrangian relaxation, doing so would require tuning a separate multiplier for each constraint, making the hyperparameter tuning process impractical at scale. To address this, we reformulate **Problem II** and present the final framework in Section 4.

4 Optimization Methods

Section 4.1 reformulates the task as a min-max optimization and adopts the γ -Gradient Descent Ascent (γ -GDA) algorithm (Schweisthal et al. 2024). To improve numerical stability, we modified the formulation and establish feasibility guarantees in Section 4.2, showing that MOSIC can identify the optimal subgroup while satisfying multiple constraints.

4.1 Min-Max Formulation and GDA

Since neither the objective nor the feasible region is convex, we first rewrite **Problem II** using the saddle point formulation in **Problem III**, converting it to a min-max problem.

 $^{{}^{1}\}hat{\phi}(x_i,a_i,y_i)$ does not depend on parameter θ as the estimation problem is separate from the parametric surrogate model S.

Algorithm 1: γ -Gradient Descent Ascent (γ -GDA)

- 1: **Input:** step size η , decay rate ζ , objective function
- 2: Randomly initialize θ_0 ;
- 3: $\lambda_0 = 0$
- 4: **for** $t = 0, 1, \dots T$ **do**
- If converged, output $\boldsymbol{\theta}^* = \boldsymbol{\theta}_t$ 5:
- 6: $\gamma \leftarrow (1+t)^{\zeta}$
- Update θ_t using gradient descent with learning rate
 $$\begin{split} & \eta/\gamma : \boldsymbol{\theta}_{t+1} \leftarrow \boldsymbol{\theta}_t - \left(\frac{\eta}{\gamma}\right) \nabla_{\boldsymbol{\theta}} L(\boldsymbol{\theta}_t, \lambda_t). \\ & \text{Update } \boldsymbol{\lambda}_t \text{ using gradient ascent with learning rate } \eta : \end{split}$$
- $\lambda_{t+1} \leftarrow \lambda_t + \bar{\eta} \bar{\nabla}_{\lambda} L(\theta_{t+1}, \lambda_t).$
- 9: end for
- 10: Output: $\boldsymbol{\theta}^T$

We then solve it by applying γ -GDA, as described in Algorithm 1. Our goal is to minimize the resulting Lagrangian, $L(\boldsymbol{\theta}, \boldsymbol{\lambda})$, associated with **Problem II**:

$$L(\boldsymbol{\theta}, \boldsymbol{\lambda}) := -f(\boldsymbol{\theta}) + \boldsymbol{\lambda}^T \boldsymbol{g}(\boldsymbol{\theta}), \tag{8}$$

where

$$\boldsymbol{\lambda} = \begin{bmatrix} \lambda_1 \\ \vdots \\ \lambda_n \\ \lambda_{n+1} \end{bmatrix}, \quad \boldsymbol{g}(\boldsymbol{\theta}) = \begin{bmatrix} S(x_1; \boldsymbol{\theta})h(x_1; \alpha) \\ \vdots \\ S(x_n; \boldsymbol{\theta})h(x_n; \alpha) \\ c - \frac{1}{n} \sum_{i=1}^n S(\boldsymbol{x}_i; \boldsymbol{\theta}) \end{bmatrix}. \quad (9)$$

For notational convenience, we write $g(\theta)$ without explicitly indicating its dependence on fixed constraint values c and α (or those for any additional constraint, if present). We solve the **primal constrained problem** directly through a minmax Lagrangian formulation, unlike Lagrangian relaxation which operates on the dual problem. This saddle-point approach preserves feasibility guarantees while avoiding the instability of dual methods under non-convex constraints. The solution to **Problem II** is equivalent to solving (Boyd and Vandenberghe 2004):

$$\min_{\boldsymbol{\theta}} \max_{\boldsymbol{\lambda} \geq 0} L(\boldsymbol{\theta}, \boldsymbol{\lambda}). \tag{Problem III}$$

We adopt γ -GDA algorithm (Jin, Netrapalli, and Jordan 2020) to solve this problem. As shown in Alrorithm 1, each iteration performs a gradient descent step on θ followed by a gradient ascent step on λ . The descent step's learning rate decays over time, as required by Theorem 1, which underpins Proposition 1 and Lemma 2.

While appearing effective, Algorithm 1 exhibits notable numerical instability. To illustrate, consider a scenario with a single group size constraint (Constraint (6)) and its Lagrange multiplier λ_{n+1} . Initially, the constraint is violated because the group size is below the threshold, leading to a positive gradient that increments λ_{n+1} at each iteration. Once the constraint is met, the gradient becomes negative, driving λ_{n+1} toward 0. However, due to the small learning rate, λ_{n+1} remains nonzero in subsequent iterations, continuing to penalize the objective and lead to artificially shrunk feasible regions. This instability extends to multiple constraints,

causing the algorithm to oscillate between a strictly feasible but suboptimal θ and an optimal but infeasible θ , undermining convergence. To address this, we introduce a modified objective in Section 4.2 and provide theoretical guarantees.

Modified Min-Max problem and Feasibility Guarantees

We make two additional modifications to **Problem III**:

- a) Deactivating the corresponding penalty term once a constraint is satisfied, and
- b) Incorporating additional penalty terms to ensure convergence to a feasible, locally optimal solution.

For a), we wrap the constraint terms with ReLU function:

$$L'(\boldsymbol{\theta}, \boldsymbol{\lambda}) = -f(\boldsymbol{\theta}) + \boldsymbol{\lambda}^T ReLU(\boldsymbol{g}(\boldsymbol{\theta})). \tag{10}$$

When $q_i(\theta) \le 0$ (i.e., the constraint is satisfied), the penalty term vanishes (i.e., $ReLU(g_i(\theta)) = 0$), preventing further penalization of the objective. This approach excludes satisfied constraints from optimization, improving stability.

For b), we begin by defining local optimality in the context of a nonconvex-nonconcave min-max problem, introducing the concept of *local minmax point* (Definition 1). We then modify the objective to ensure that Algorithm 1 converges to a local minmax point (Proposition 1). Finally, we establish the feasibility of the returned solution in Lemma 2.

A local minmax point (Definition 1), informally, is a fixed point where the objective remains stable under small perturbations in θ (the parameters over which we minimize) and worst-case perturbations in λ (the parameters over which we maximize). Theorem 1 (Jin, Netrapalli, and Jordan 2020) states that if the min-max objective function is twice differentiable, then the γ -GDA algorithm, upon convergence, reaches either a local minmax point or a stationary point with a degenerate (i.e., not invertible) Hessian.

However, the Hessian of our objective in Equation (10) is inherently degenerate: $\nabla^2_{\lambda\lambda}L(\theta,\lambda) = 0$. This degeneracy prevents us from proving that the algorithm converges to local minmax points, and further, hinders our ability to guarantee the feasibility of the resulting solution. Unlike Nandwani et al. (2019), who did not exclude degenerate pointspotentially invalidating their results-we introduce a modification, as shown below, to eliminates degenerate points, leading to the final optimization objective of MOSIC:

$$\tilde{L}(\boldsymbol{\theta}, \boldsymbol{\lambda}) = -f(\boldsymbol{\theta}) + \boldsymbol{\lambda}^T ReLU(\boldsymbol{g}(\boldsymbol{\theta})) - \frac{\beta}{2} \boldsymbol{\lambda}^2.$$
 (11)

Now our problem reduces to solving **Problem IV**:

$$\min_{\boldsymbol{\theta}} \max_{\boldsymbol{\lambda} > 0} \tilde{L}(\boldsymbol{\theta}, \boldsymbol{\lambda}).$$
 (Problem IV

With this update, we establish that, if Algorithm 1 converges, it converges to a strict local minmax point:

Proposition 1 (Local Optimality). Let (θ', λ') be a linearly stable point (formally defined in Definition 2) of Algorithm 1. Then, (θ', λ') must be a strict local minmax point.

The proof of Proposition 1 (Appendix B.2) relaxes the twice-differentiability requirement in Theorem 1, and shows that the algorithm cannot converge to degenerate points. Building on this, the following result, Lemma 2, shows that upon convergence, all constraints are approximately satisfied within a small tolerance. This guarantee applies not only to the group size constraint but also to arbitrary linear constraints, which include the overlap constraint.

Lemma 2. Let (θ^*, λ^*) be a strict local min-max point obtained by Algorithm 1. Suppose the constraint set includes:

- a group size constraint: $g^{\text{size}}(\boldsymbol{\theta}) = c \frac{1}{n} \sum_{i=1}^{n} S(x_i; \boldsymbol{\theta}),$ and $K(K \geq 0)$ additional linear constraints of the form: $g^k(\boldsymbol{\theta}) = a^k + \sum_{i=1}^{n} b_i^k S(x_i; \boldsymbol{\theta}),$

which together define the constraint vector:

$$g(\boldsymbol{\theta}) := \begin{bmatrix} a^1 + \sum_{i=1}^n b_i^1 S(x_i; \boldsymbol{\theta}) \\ \vdots \\ a^K + \sum_{i=1}^n b_i^K S(x_i; \boldsymbol{\theta}) \\ c - \frac{1}{n} \sum_{i=1}^n S(x_i; \boldsymbol{\theta}) \end{bmatrix},$$

where $a^k, b_i^k \in \mathbb{R}$, and, $\forall k, |\sum_{i=1}^n b_i^k| > 0$. Suppose β satisfies:

$$\beta < \frac{\xi(c-\xi)|\mu_{\Delta}|}{2\phi_{\max}L},$$

where $\xi>0$ is a small tolerance error; $\phi_{\max}=\max_i\hat{\phi}(x_i,a_i,y_i)$; $L=\sup|\frac{\partial S(\cdot;\boldsymbol{\theta})}{\partial \theta_j}|$, the coordinate-wise Lipschitz constant of $S(\cdot; \boldsymbol{\theta})$, $\mu_{\Delta} = \mathbb{E} \frac{\partial S(x_i; \boldsymbol{\theta})}{\partial \theta_i}$, and j = $\arg\max_{L} \frac{|\mu_{\Delta}|}{L}$.

Then one of the following holds:

- 1. Model collapse: $\frac{1}{n} \sum_{i=1}^{n} S(x_i; \boldsymbol{\theta}^*) < \xi$.
- 2. Each constraint is approximately satisfied. For the group size constraint,

$$q^{size}(\boldsymbol{\theta}^*) < \xi$$
.

For the k-th linear constraint, with probability at least $1-\delta$.

$$g^{k}(\boldsymbol{\theta}^{*}) \leq \frac{\xi}{|\sum_{i=1}^{n} b_{i}^{k}| \left(1 + \frac{L}{|\mu_{\lambda}| \sqrt{n}} \sqrt{\log \frac{2}{\delta}}\right)}.$$

The proof of Lemma 2 (Appendix B.3) analyzes each constraint at strict local minmax points and establishes that, with β properly chosen,² the constraints are either fully satisfied or violated up to a small tolerance error, if the model does not collapse. The proof further shows that, as long as the feasible region is non-negligible, the model is unlikely to collapse. In practice, if the model converges to a near-zero subgroup size, the run is restarted using a different random seed. Persistent collapse suggests that the feasible region defined by the multiple constraints should be carefully re-evaluated.

Algorithm 2: MOSIC

- 1: Input: $\{(\boldsymbol{x_i}, a_i, y_i)\}_{i=1}^n$, constraint-related values c and α , learning rate η , decay rate ζ
- 2: // Estimate nuisance functions
- 3: Estimate $\hat{\mu}_0(\boldsymbol{X})$ and $\hat{\mu}_1(\boldsymbol{X})$ (optional)
- 4: Estimate $\hat{e}(\boldsymbol{X})$
- 5: Compute $\hat{\phi}(\boldsymbol{x}_i, a_i, y_i)$ using nuisance functions
- 6: // Solve **Problem IV** using γGDA algorithm
- 7: Construct $\tilde{L}(\boldsymbol{\theta}; \boldsymbol{\lambda}; c, \alpha)$
- 8: $\theta^* \leftarrow \gamma$ -GDA $(\eta, \zeta, \tilde{L}(\theta; \lambda; c, \alpha))$ (Solve using Algorithm 1)
- 9: **Output:** Parametric surrogate model $S(X; \theta^*)$

Remark 1 (Implication on the overlap constraint). When $n \to \infty$, the bound on constraint violation is governed by $|\sum_{i=1}^{n} b_i^k|$. For the overlap constraint on sample j, we set $b_i^k = \mathbb{1}(i=j)h(x_j;\alpha)$, which gives $\sum_{i=1}^{n} b_i^k = h(x_j;\alpha)$. When $h(x_j;\alpha)$ is small, this denominator inflates the bound, suggesting potentially high violation. However, a small $h(x_i; \alpha)$ indicates that the corresponding violation of the overlap condition is itself negligible. Thus, such constraints can be safely ignored in practice.

Remark 2 (Extension to ratio constraints). Because the model maximizes the subgroup ATE, it naturally favors smaller subgroups by excluding samples with relatively low estimated CATE, while the group size constraint enforces a group size lower bound c. As a result, the group size typically converges to the size threshold c, i.e., $\sum_{i=1}^{n} S(x_i; \theta) \approx c$ at termination. This observation allows us to extend the linear constraint to ratio constraints

$$g^k(\boldsymbol{\theta}) = a^k + \frac{\sum_{i=1}^n b_i^k S(\boldsymbol{x_i}; \boldsymbol{\theta})}{\sum_{i=1}^n S(\boldsymbol{x_i}; \boldsymbol{\theta})}.$$

To retain compatibility with Lemma 2, we block gradient flow through the denominator during backpropagation, effectively treating it as a constant.

The linear and ratio families capture many practical constraints relevant to healthcare applications. Linear constraints include the overlap constraint and budget constraints (each patient incurs a treatment cost under limited resources). Ratio constraints cover safety constraints (e.g., risk levels associated with patients) and fairness constraints. Section 5.4 assesses MOSIC's extendability to these constraints. Due to the nonconvexity of both the objective and the feasible region, extending the guarantee to more complex constraints remains an open direction for future work.

Finally, we summarize our overall framework, MOSIC, in Algorithm 2. It first estimates the nuisances and computes the pseudo-outcomes for each sample, which are then fed into the objective function (**Problem IV**). The optimization is subsequently performed using the γ -GDA algorithm.

Experiments

We evaluate MOSIC on both synthetic and real-world data. Section 5.1 describes the datasets, and Section 5.2 outlines

²In practice, relaxing β does not substantially increase constraint violation. We recommend setting β between 10^{-5} and 0.01.

Dataset	n	d	Y
Synthetic	5,000	10	Continuous
eICU	13,361	23	Binary, Survival
MIMIC-IV	6,516	23	Binary, Survival

Table 1: Summary of data sets. n: sample size; d: data dimension; Y: outcome.

the experimental setup. Results in Section 5.3 demonstrate that MOSIC achieves high ATE while maintaining comparable covariate balance, or vice versa. Finally, Section 5.4 presents ablation studies, highlighting that MOSIC outperforms baselines under the same interpretability requirement and can be extended to multiple additional constraints.

5.1 Datasets

Synthetic Data We generate synthetic data following a procedure adapted from Assaad et al. (2021) (details in Appendix C.2). We introduce an *imbalance parameter* $\tilde{\omega} \geq 0$ to determine the strength of confounding bias. In particular, we generated two datasets with (1) no confounding bias ($\tilde{\omega} = 0$); and (2) high confounding bias ($\tilde{\omega} = 5$).

Real-World Data We use two datasets of de-identified health records from intensive care units (ICU): eICU (Pollard et al. 2018) and MIMIC-IV (Johnson et al. 2023). Our study focuses on evaluating the effectiveness of Glucocorticoids in treating sepsis patients in the ICU. The treated group (A=1) consists of patients who received an initial Glucocorticoids dose of 160mg within 10 hours before to 24 hours after ICU admission. The outcome Y represents 7-day survival, with Y=1 indicating survival and Y=0 otherwise. The input X contains baseline covariates, including lab test results, vital signs, and sequential organ failure assessment (SOFA) scores (Vincent et al. 1996).

5.2 Setups

Baselines We compare MOSIC with two categories from Section 2: Those designed for subgroup identification and those adapted from CATE estimation algorithms.

- Dedicated subgroup identification methods: We evaluate

 (1) CAPITAL,
 (2) OWL, and
 (3) VT, modifying them to incorporate a group size constraint via thresholding (Details in Appendix C.3). These methods prioritize interpretability, making it unclear whether performance limits stem from this trade-off or poor CATE estimation. To address this, we consider the next category of benchmarks.
- CATE estimation algorithms: We evaluate three methods: (1) CT, (2) CF, (3) Dragonnet. Patients are ranked by the estimated CATE values and the top subgroup of the desired size is selected (VanderWeele et al. 2019). Although these methods are not designed for subgroup identification, they serve as a natural baseline. If CATE estimation were accurate, this approach would identify the optimal subgroup, allowing us to separate the impact of estimation reliability from the interpretability trade-off.

Evaluation Metrics We assess performance using two metrics: 1) Subgroup ATE, which measures whether identified subgroups achieve high ATE at the desired size (using ground-truth ATE for synthetic data and the difference between subgroup and overall AIPTW estimates for real-world data). 2) ATE Estimation Reliability measures the AIPTW estimation error on synthetic data and the number of unbalanced features on real-world data because the ground truth ATE is not observed. Although MOSIC can enforce the overlap constraint on the training set by design (Figure E.3.1), directly evaluating constraint violations on the test set is less meaningful under distribution shifts. Instead, we assess ATE estimation reliability, which captures the intended effect of the overlap constraint.

A feature is considered unbalanced (Cohen 2013) if its standardized mean difference (SMD) > 0.2 after IPTW-reweighting (Austin 2009; Zang et al. 2023). A higher number of unbalanced features indicates larger estimation uncertainty and lower reliability of the subgroup. To validate feature imbalance as a proxy for estimation error, we further report the feature imbalance in synthetic data (Figure E.3.1).

Implementation Details For all datasets, we perform 100 random splits of the training and test sets. For each split, we first conduct a 5-fold cross-validation on the training set to determine the optimal hyperparameters (see Appendix C.5 for details). The model is then retrained on the entire training set using the selected hyperparameters and evaluated on the corresponding test set. The final results are reported using the mean and standard deviations across all 100 evaluations.

We implement the subgroup identification model (S) using MLP and DT. In the next sections, 'MOSIC' refers to MOSIC-MLP, unless stated otherwise. Following (Marton et al. 2024), we represent the DT as a neural network. These models are trained using Algorithm 1, with L1 regularization applied in the loss function. For nuisance function estimation, we use LR for the propensity score model $\hat{e}(\cdot)$, and Dragonnet for the outcome models $\hat{\mu}_a(\cdot)$ (Appendix C.4). ³

5.3 Results

Synthetic Data To assess the impact of overlap constraints, we compare MOSIC with ($\alpha=0.02$) and without ($\alpha=0$) them. Figure 1 and Figure E.1.1 present results from the confounded and unconfounded synthetic data. Compared with baselines, the left column indicates that MOSIC consistently identifies subgroups with the highest ATE across all group sizes, and the right column shows that it achieves the lowest ATE estimation errors.

Further, we numerically verify that MOSIC can indeed satisfy the overlap constraint and investigate the correlation between the estimation error and the number of unbalanced features (Figure E.3.1). We also investigate the statistical properties of the proposed procedure in Appendix F and G.

Real-World Data Figures 2 demonstrates that MOSIC consistently outperforms other methods. We highlight the

³Empirically, estimating propensity scores with Dragonnet results in a large number of unbalanced features; we therefore adopt LR, demonstrating the flexibility of MOSIC.

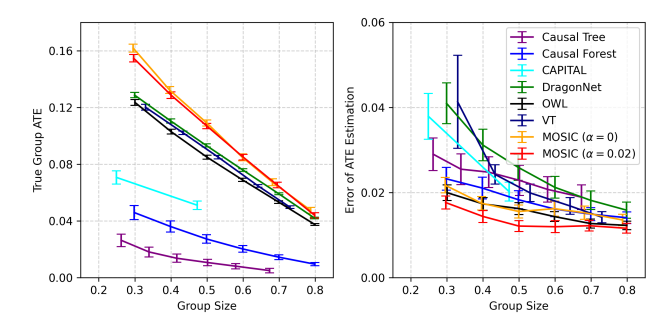


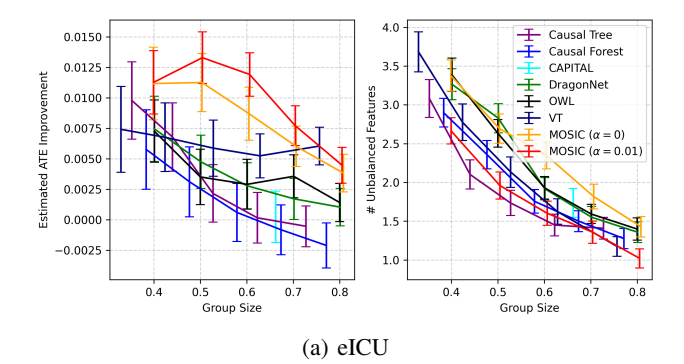
Figure 1: True ATE and ATE estimation error across different group sizes on confounded synthetic data($\omega = 5$).

importance of jointly evaluating subgroup ATE and covariate balance when assessing performance. A large ATE alone is insufficient if covariate imbalance persists, as it may indicate unreliable estimates. As shown in Figures 2 (left), MOSIC achieves higher subgroup ATEs at comparable group sizes in most cases. In scenarios where the ATE advantage is not statistically significant (e.g., MOSIC ($\alpha=0.01$) vs. CF at c=0.6 on MIMIC, p = 0.68), MOSIC still exhibits improved covariate balance (e.g., MOSIC ($\alpha=0.01$) vs. CF at c=0.6 on MIMIC, p = 0.000052). Full statistical test results are provided in Appendix D. Additionally, the overlap constraint in MOSIC significantly improves covariate balance on eICU (Figures 2(a), right).

5.4 Ablation Studies

Decision Tree as Base Model While MOSIC-MLP achieves stronger performance than the baselines, its blackbox nature limits interpretability. In contrast, decision trees are favored in clinical settings for their transparency, allowing stakeholders to understand and trust subgroup recommendations (Cai et al. 2022). We compare MOSIC with DT implementation to other DT-based baselines (CT, CF) on eICU. VT is excluded due to its high ATE estimation error on synthetic data (Figure 1). To impose equal interpretability requirement, we fix the tree depth to 5 for both MOSIC (denoted as MOSIC-DT) and CT, and use ensembles of 3 trees of depth 5 for MOSIC (denoted as MOSIC-Forest) and CF. As shown in Figure E.2.1, MOSIC consistently outperforms CT and CF under the same interpretability requirement. Notably, despite the limited model capacity, MOSIC effectively enforces both group size and overlap constraints, leading to improved covariate balance.

Extension to Additional Constraints While this study focuses on the group size and overlap constraints, MOSIC can be readily extended to multiple constraints. To illustrate, we experimented on synthetic data to progressively enforce safety, budget, and fairness constraints (Appendix E.4). We also experimented on eICU to discourage the selection of patients with injured central nervous system (CNS), as studies have shown that glucocorticoids may exacerbate neural



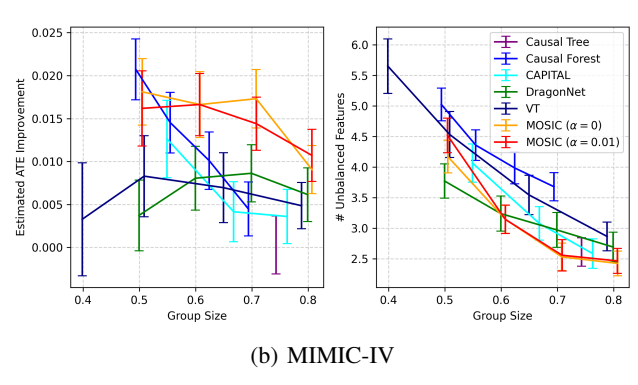


Figure 2: Estimated ATE and the number of unbalanced features across different group sizes for real-world datasets.⁴

damage (Hill and Spencer-Segal 2021). Specifically, we required that the proportion of patients with a Glasgow Coma Scale (GCS) score < 6 remain below 0.05. A GCS< 6 corresponds to the most severe CNS dysfunction in the SOFA measurement, a widely used ICU metric. This constraint was applied in addition to the group size constraint (c=0.4) and overlap constraint ($\alpha=0.01$). Table 2 and Appendix E.5 demonstrate that MOSIC can additionally satisfy this safety constraint. The findings demonstrate that MOSIC can effectively accommodate multiple constraints simultaneously.

Table 2: eICU with GCS score constraint

Metric	before	after
Group Size	0.46 ± 0.10	0.44 ± 0.10
# Unbalanced Features	2.0 ± 1.72	2.2 ± 2.28
ATE Improvement	0.02 ± 0.02	0.02 ± 0.02
Proportion of GCS< 6	0.15 ± 0.05	0.03 ± 0.03

^{*}Values are mean±standard error across 100 random splits.

6 Conclusion

We propose MOSIC, a model-agnostic framework for optimal subgroup identification that handles multiple constraints with feasibility guarantees. It demonstrates strong empirical performance under group size and overlap constraints, flexibly extends to additional clinical constraints, and supports diverse models to deliver interpretable solutions.

⁴The OWL method failed to converge on the MIMIC-IV dataset and was therefore omitted from the figure.

References

- Assaad, S.; Zeng, S.; Tao, C.; Datta, S.; Mehta, N.; Henao, R.; Li, F.; and Carin, L. 2021. Counterfactual representation learning with balancing weights. In *International Conference on Artificial Intelligence and Statistics*, 1972–1980. PMLR.
- Athey, S.; and Imbens, G. 2016. Recursive partitioning for heterogeneous causal effects. *Proceedings of the National Academy of Sciences*, 113(27): 7353–7360.
- Athey, S.; and Wager, S. 2021. Policy learning with observational data. *Econometrica*, 89(1): 133–161.
- Austin, P. C. 2009. Using the standardized difference to compare the prevalence of a binary variable between two groups in observational research. *Communications in statistics-simulation and computation*, 38(6): 1228–1234.
- Boyd, S.; Parikh, N.; Chu, E.; Peleato, B.; Eckstein, J.; et al. 2011. Distributed optimization and statistical learning via the alternating direction method of multipliers. *Foundations and Trends*® *in Machine learning*, 3(1): 1–122.
- Boyd, S.; and Vandenberghe, L. 2004. *Convex optimization*. Cambridge university press.
- Cai, H.; Lu, W.; Marceau West, R.; Mehrotra, D. V.; and Huang, L. 2022. CAPITAL: Optimal subgroup identification via constrained policy tree search. *Statistics in medicine*, 41(21): 4227–4244.
- Cai, T.; Tian, L.; Wong, P. H.; and Wei, L.-J. 2011. Analysis of randomized comparative clinical trial data for personalized treatment selections. *Biostatistics*, 12(2): 270–282.
- Chernozhukov, V.; Chetverikov, D.; Demirer, M.; Duflo, E.; Hansen, C.; Newey, W.; and Robins, J. 2018. Double/debiased machine learning for treatment and structural parameters.
- Cohen, J. 2013. *Statistical power analysis for the behavioral sciences*. routledge.
- Cole, S. R.; and Hernán, M. A. 2008. Constructing inverse probability weights for marginal structural models. *American journal of epidemiology*, 168(6): 656–664.
- Crump, R. K.; Hotz, V. J.; Imbens, G. W.; and Mitnik, O. A. 2009. Dealing with limited overlap in estimation of average treatment effects. *Biometrika*, 96(1): 187–199.
- Doubleday, K.; Zhou, J.; Zhou, H.; and Fu, H. 2022. Risk controlled decision trees and random forests for precision Medicine. *Statistics in medicine*, 41(4): 719–735.
- Dusseldorp, E.; Doove, L.; and Mechelen, I. v. 2016. Quint: An R package for the identification of subgroups of clients who differ in which treatment alternative is best for them. *Behavior research methods*, 48: 650–663.
- Foster, J. C.; Taylor, J. M.; and Ruberg, S. J. 2011. Subgroup identification from randomized clinical trial data. *Statistics in medicine*, 30(24): 2867–2880.
- Gao, W.; Goldfarb, D.; and Curtis, F. E. 2020. ADMM for multiaffine constrained optimization. *Optimization Methods and Software*, 35(2): 257–303.
- Gruber, S.; Phillips, R. V.; Lee, H.; and van der Laan, M. J. 2022. Data-Adaptive Selection of the Propensity Score

- Truncation Level for Inverse-Probability—Weighted and Targeted Maximum Likelihood Estimators of Marginal Point Treatment Effects. *American Journal of Epidemiology*, 191(9): 1640–1651.
- Hill, A. R.; and Spencer-Segal, J. L. 2021. Glucocorticoids and the brain after critical illness. *Endocrinology*, 162(3): bqaa242.
- Huang, X.; Sun, Y.; Trow, P.; Chatterjee, S.; Chakravartty, A.; Tian, L.; and Devanarayan, V. 2017. Patient subgroup identification for clinical drug development. *Statistics in medicine*, 36(9): 1414–1428.
- Jin, C.; Netrapalli, P.; and Jordan, M. 2020. What is Local Optimality in Nonconvex-Nonconcave Minimax Optimization? In III, H. D.; and Singh, A., eds., *Proceedings of the 37th International Conference on Machine Learning*, volume 119 of *Proceedings of Machine Learning Research*, 4880–4889. PMLR.
- Johnson, A. E.; Bulgarelli, L.; Shen, L.; Gayles, A.; Shammout, A.; Horng, S.; Pollard, T. J.; Hao, S.; Moody, B.; Gow, B.; et al. 2023. MIMIC-IV, a freely accessible electronic health record dataset. *Scientific data*, 10(1): 1.
- Kallus, N. 2020. More Efficient Policy Learning via Optimal Retargeting. arXiv:1906.08611.
- Kiriakidou, N.; and Diou, C. 2022. An evaluation framework for comparing causal inference models. In *Proceedings of the 12th Hellenic Conference on Artificial Intelligence*, 1–9.
- Kosorok, M. R.; and Laber, E. B. 2019. Precision medicine. *Annual review of statistics and its application*, 6(1): 263–286.
- Kravitz, R. L.; Duan, N.; and Braslow, J. 2004. Evidence-based medicine, heterogeneity of treatment effects, and the trouble with averages. *The Milbank Quarterly*, 82(4): 661–687.
- Künzel, S. R.; Sekhon, J. S.; Bickel, P. J.; and Yu, B. 2019. Metalearners for estimating heterogeneous treatment effects using machine learning. *Proceedings of the national academy of sciences*, 116(10): 4156–4165.
- Lacoste-Julien, S. 2016. Convergence rate of frank-wolfe for non-convex objectives. *arXiv preprint arXiv:1607.00345*.
- Lipkovich, I.; Dmitrienko, A.; Denne, J.; and Enas, G. 2011. Subgroup identification based on differential effect search—a recursive partitioning method for establishing response to treatment in patient subpopulations. *Statistics in medicine*, 30(21): 2601–2621.
- Lipkovich, I.; Svensson, D.; Ratitch, B.; and Dmitrienko, A. 2024. Modern approaches for evaluating treatment effect heterogeneity from clinical trials and observational data. *Statistics in Medicine*, 43(22): 4388–4436.
- Liu, Y.; Wang, Y.; Kosorok, M. R.; Zhao, Y.; and Zeng, D. 2018. Augmented outcome-weighted learning for estimating optimal dynamic treatment regimens. *Statistics in medicine*, 37(26): 3776–3788.
- Marton, S.; Lüdtke, S.; Bartelt, C.; and Stuckenschmidt, H. 2024. GradTree: Learning axis-aligned decision trees with gradient descent. In *Proceedings of the AAAI Conference on Artificial Intelligence*, volume 38, 14323–14331.

Mehrabi, N.; Morstatter, F.; Saxena, N.; Lerman, K.; and Galstyan, A. 2021. A survey on bias and fairness in machine learning. *ACM computing surveys (CSUR)*, 54(6): 1–35.

Nandwani, Y.; Pathak, A.; Mausam; and Singla, P. 2019. A primal-dual formulation for deep learning with constraints. In *Proceedings of the 33rd International Conference on Neural Information Processing Systems*, 12179–12190.

Pollard, T. J.; Johnson, A. E.; Raffa, J. D.; Celi, L. A.; Mark, R. G.; and Badawi, O. 2018. The eICU Collaborative Research Database, a freely available multi-center database for critical care research. *Scientific data*, 5(1): 1–13.

Qiu, H.; Carone, M.; and Luedtke, A. 2022. Individualized treatment rules under stochastic treatment cost constraints. *Journal of causal inference*, 10(1): 480–493.

Robins, J. M.; Rotnitzky, A.; and Zhao, L. P. 1995. Analysis of semiparametric regression models for repeated outcomes in the presence of missing data. *Journal of the american statistical association*, 90(429): 106–121.

Schweisthal, J.; Frauen, D.; Melnychuk, V.; and Feuerriegel, S. 2024. Reliable off-policy learning for dosage combinations. In *Proceedings of the 37th International Conference on Neural Information Processing Systems*, NIPS '23. Red Hook, NY, USA: Curran Associates Inc.

Shalit, U.; Johansson, F. D.; and Sontag, D. 2017. Estimating individual treatment effect: generalization bounds and algorithms. In *International conference on machine learning*, 3076–3085. PMLR.

Shi, C.; Blei, D.; and Veitch, V. 2019. Adapting neural networks for the estimation of treatment effects. *Advances in neural information processing systems*, 32.

Tesei, G.; Giampanis, S.; Shi, J.; and Norgeot, B. 2023. Learning end-to-end patient representations through self-supervised covariate balancing for causal treatment effect estimation. *Journal of Biomedical Informatics*, 140: 104339.

Van Der Laan, M. J.; and Rubin, D. 2006. Targeted maximum likelihood learning. *The international journal of biostatistics*, 2(1).

VanderWeele, T. J.; Luedtke, A. R.; van der Laan, M. J.; and Kessler, R. C. 2019. Selecting optimal subgroups for treatment using many covariates. *Epidemiology*, 30(3): 334–341.

Vincent, J. L.; Moreno, R.; Takala, J.; Willatts, S.; De Mendonça, A.; Bruining, H.; Reinhart, C.; Suter, P.; and Thijs, L. G. 1996. The SOFA (Sepsis-related Organ Failure Assessment) score to describe organ dysfunction/failure: On behalf of the Working Group on Sepsis-Related Problems of the European Society of Intensive Care Medicine (see contributors to the project in the appendix).

Wager, S.; and Athey, S. 2018. Estimation and inference of heterogeneous treatment effects using random forests. *Journal of the American Statistical Association*, 113(523): 1228–1242.

Wang, T.; and Rudin, C. 2021. Causal Rule Sets for Identifying Subgroups with Enhanced Treatment Effect. arXiv:1710.05426.

Wang, Y.; Yin, W.; and Zeng, J. 2019. Global convergence of ADMM in nonconvex nonsmooth optimization. *Journal of Scientific Computing*, 78: 29–63.

Zang, C.; Zhang, H.; Xu, J.; Zhang, H.; Fouladvand, S.; Havaldar, S.; Cheng, F.; Chen, K.; Chen, Y.; Glicksberg, B. S.; et al. 2023. High-throughput target trial emulation for Alzheimer's disease drug repurposing with real-world data. *Nature communications*, 14(1): 8180.

Zhao, Y.; Zeng, D.; Rush, A. J.; and Kosorok, M. R. 2012. Estimating individualized treatment rules using outcome weighted learning. *Journal of the American Statistical Association*, 107(499): 1106–1118.

Zhou, J.; Yang, L.; Liu, X.; Gu, X.; Sun, L.; and Chen, W. 2024. CURLS: Causal Rule Learning for Subgroups with Significant Treatment Effect. In *Proceedings of the 30th ACM SIGKDD Conference on Knowledge Discovery and Data Mining*, KDD '24, 4619–4630. New York, NY, USA: Association for Computing Machinery. ISBN 9798400704901.

A Preliminary Definitions and Theorems

A.1 Local minmax point

Definition 1 (Local minmax point). A point (θ^*, λ^*) is said to be a local minmax point of L, if there exists $\delta_0 > 0$ and a continuous function h satisfying $h(\delta) \to 0$ as $\delta \to 0$, such that for any $\delta \leq \delta_0$, and any (θ, λ) satisfying

$$\|\theta - \theta^*\| \le \delta$$
 and $\|\lambda - \lambda^*\| \le h(\delta)$,

we have

$$L(\theta^{\star}, \lambda) \le L(\theta^{\star}, \lambda^{\star}) \le \max_{\lambda': \|\lambda' - \lambda^{\star}\| \le h(\delta)} L(\theta, \lambda').$$

If a point (θ^*, λ^*) *satisfy*

$$\left[\nabla_{\theta\theta}^2 L - \nabla_{\theta\lambda}^2 L (\nabla_{\lambda\lambda}^2 L)^{-1} \nabla_{\lambda\theta}^2 L\right] > 0,$$

we call it a strict local minmax point (Jin, Netrapalli, and Jordan 2020).

A.2 Linearly Stable Point

Definition 2 (Linearly Stable Point). For a differentiable dynamical system \mathbf{w} , a fixed point \mathbf{z}^{\star} is a linearly stable point of \mathbf{w} if its Jacobian matrix $\mathbf{J}(\mathbf{z}^{\star}) := \left(\frac{\partial \mathbf{w}}{\partial \mathbf{z}}\right)(\mathbf{z}^{\star})$ has spectral radius $\rho(\mathbf{J}(\mathbf{z}^{\star})) \leq 1$.

A.3 Convergence of γ -GDA algorithm

Theorem 1. (Jin et al (Jin, Netrapalli, and Jordan 2020), Theorem 26): Given an objective: $\min_{x \text{ in} \mathcal{X}} \max_{y \in \mathcal{Y}} f(x, y)$. For any twice-differentiable f, the strict linearly stable limit points of the γ -GDA flow are $\{\text{strict local minmax points}\} \cup \{(\theta, \lambda) - (\theta, \lambda) \text{ is stationary and } \nabla^2_{\lambda\lambda} f(\theta, \lambda) \text{ is degenerate}\} \text{ as } \gamma \to \infty$.

B Proofs

B.1 Proof of Lemma 1

Lemma 1. $S(\boldsymbol{x}_i;\boldsymbol{\theta})h(\boldsymbol{x}_i,\alpha) \leq 0$ if and only if $\alpha \leq \hat{e}(\boldsymbol{x}_i) \leq$

Proof. We proceed by proving both directions separately. Forward Direction: Suppose $S(x_i; \theta)h(x_i) \leq 0$. We aim to show that this implies $\alpha \leq e(x_i) \leq 1 - \alpha$.

$$S(x_i;\theta)h(x_i) \leq 0$$

$$\Rightarrow h(x_i) \leq 0 \quad \text{(Since } S(x_i) > 0)$$

$$\Rightarrow 1 - \frac{e(x_i)(1 - e(x_i))}{\alpha(1 - \alpha)} \leq 0 \quad \text{(Substituting } h(x_i))$$

$$\Rightarrow \alpha(1 - \alpha) - e(x_i)(1 - e(x_i)) \leq 0$$

$$\Rightarrow e(x_i) - \alpha - (e(x_i)^2 - \alpha^2) \geq 0$$

$$\Rightarrow (e(x_i) - \alpha)(1 - (e(x_i) + \alpha)) \geq 0$$

$$\Rightarrow (e(x_i) - \alpha)(1 - \alpha - e(x_i)) \geq 0$$

$$\Rightarrow \alpha \leq e(x_i) \leq 1 - \alpha.$$

Backward Direction: Suppose $\alpha \leq e(x_i) \leq 1 - \alpha$. We need to show that this implies $S(x_i; \theta)h(x_i) \leq 0$.

Define the auxiliary function q(z) = z(1-z), whose derivative is given by:

$$q'(z) = 1 - 2z.$$

Thus, q(z) attains its maximum at z = 0.5.

When $0 < \alpha \le e(x_i) \le 0.5$, we have $q'(e(x_i)) = 1$ $2e(x_i) \geq 0$, which implies that $q(e(x_i))$ is non-decreasing on [0, 0.5]. Consequently, from the assumption $\alpha \leq e(x_i)$, we obtain:

$$q(e(x_i)) \ge q(\alpha) \implies e(x_i)(1 - e(x_i)) \ge \alpha(1 - \alpha).$$

- Similarly, for $0.5 < e(x_i) \le 1 - \alpha < 1$, we have $e(x_i)(1 - \alpha) \le 1 - \alpha < 1$ $e(x_i) \ge \alpha (1 - \alpha).$

By combining both cases, we conclude that:

$$e(x_i)(1 - e(x_i)) \ge \alpha(1 - \alpha).$$

Dividing both sides by $\alpha(1-\alpha)$ yields:

$$1 - \frac{e(x_i)(1 - e(x_i))}{\alpha(1 - \alpha)} = h(x_i) \le 0.$$

Since $S(x_i) > 0$, it follows that:

$$S(x_i)h(x_i) \leq 0.$$

This completes the proof.

B.2 Proof of Proposition 1

Proposition 1 (Local Optimality). Let (θ', λ') be a linearly stable point (formally defined in Definition 2) of Algorithm 1. Then, (θ', λ') must be a strict local minmax point.

Proof. The derivation of Theorem 1 relies on the Jacobian matrix and requires twice differentiability. However, our objective function incorporates ReLU activations, introducing

non-differentiability at the origin. This prevents us from directly applying Theorem 1 in its standard form. Nonetheless, since the probability of encountering exact zero inputs to ReLU is negligible, our objective function remains effectively differentiable in practice when using gradient-based optimization.

Thus, the key arguments of Theorem 1 extend to our objective (Problem IV), implying that its stable limit points must either be local minmax points or points where the second derivative is degenerate.

Further, we compute the first and second derivatives of Lwith respect to λ :

$$\frac{\partial L}{\partial \lambda_i} = \text{ReLU}(g_i(\theta)) - \beta \lambda_i, \tag{12}$$

$$\frac{\partial^2 L}{\partial \lambda_i \lambda_j} = \begin{cases} 0 & \text{if } i \neq j, \\ -\beta & \text{if } i = j. \end{cases}$$
 (13)

Since $\beta > 0$, the Hessian matrix $\frac{\partial^2 L}{\partial \lambda_i \lambda_i}$ is never degenerate. Applying Theorem 2, we conclude that the strict linearly stable limit points of the γ -GDA flow are precisely the set of local minmax points.

B.3 Proof of Lemma 2

Lemma 2. Let (θ^*, λ^*) be a strict local min-max point obtained by Algorithm 1. Suppose the constraint set includes:

- a group size constraint: $g^{\text{size}}(\boldsymbol{\theta}) = c \frac{1}{n} \sum_{i=1}^{n} S(x_i; \boldsymbol{\theta}),$ and $K(K \geq 0)$ additional linear constraints of the form: $g^k(\boldsymbol{\theta}) = a^k + \sum_{i=1}^{n} b_i^k S(x_i; \boldsymbol{\theta}),$

which together define the constraint vector:

$$\boldsymbol{g}(\boldsymbol{\theta}) := \begin{bmatrix} a^1 + \sum_{i=1}^n b_i^1 S(x_i; \boldsymbol{\theta}) \\ \vdots \\ a^K + \sum_{i=1}^n b_i^K S(x_i; \boldsymbol{\theta}) \\ c - \frac{1}{n} \sum_{i=1}^n S(x_i; \boldsymbol{\theta}) \end{bmatrix},$$

where $a^k, b_i^k \in \mathbb{R}$, and, $\forall k, |\sum_{i=1}^n b_i^k| > 0$. Suppose β satisfies:

$$\beta < \frac{\xi(c-\xi)|\mu_{\Delta}|}{2\,\phi_{\max}L},$$

where $\xi > 0$ is a small tolerance error; $\phi_{max} =$ $\max_{i} \hat{\phi}(x_i, a_i, y_i); L = \sup_{i} |\frac{\partial S(\cdot; \boldsymbol{\theta})}{\partial \theta_j}|, the coordinate-wise$ Lipschitz constant of $S(\cdot; \boldsymbol{\theta})$, $\mu_{\Delta} = \mathbb{E} \frac{\partial S(x_i; \boldsymbol{\theta})}{\partial \theta_i}$, and j = $\arg\max \frac{|\mu_{\Delta}|}{I}$.

Then one of the following holds:

- 1. Model collapse: $\frac{1}{n} \sum_{i=1}^{n} S(x_i; \boldsymbol{\theta}^*) < \xi$. 2. Each constraint is approximately satisfied. For the group size constraint,

$$g^{size}(\boldsymbol{\theta}^*) \leq \xi$$
.

For the k-th linear constraint, with probability at least

$$g^{k}(\boldsymbol{\theta}^{*}) \leq \frac{\xi}{|\sum_{i=1}^{n} b_{i}^{k}| \left(1 + \frac{L}{|\mu_{\Delta}|\sqrt{n}} \sqrt{\log \frac{2}{\delta}}\right)}.$$

Proof. At convergence, the following condition holds:

$$\left. \frac{\partial L}{\partial \boldsymbol{\lambda}} \right|_{\boldsymbol{\lambda} = \boldsymbol{\lambda}^*} = ReLU(\boldsymbol{g}(\boldsymbol{\theta}^*)) - \beta \boldsymbol{\lambda}^* = \boldsymbol{0}, \quad (14)$$

$$\frac{\partial L}{\partial \boldsymbol{\theta}}\Big|_{\boldsymbol{\theta} = \boldsymbol{\theta}^*} = -\frac{\partial f}{\partial \boldsymbol{\theta}}\Big|_{\boldsymbol{\theta} = \boldsymbol{\theta}^*} + \boldsymbol{\lambda}^* \frac{\partial ReLU}{\partial \boldsymbol{g}} \cdot \frac{\partial \boldsymbol{g}}{\partial \boldsymbol{\theta}}\Big|_{\boldsymbol{\theta} = \boldsymbol{\theta}^*} = \boldsymbol{0} \ \ (15)$$

Since Eq. (14) applied component-wise to $g(\theta^*)$, we analyze each individual component $g(\theta^*)$ separately. Due to ReLU, we distinguish between two cases: $g(\theta^*) \leq 0$ and $g(\theta^*) > 0$. When $g(\theta^*) \leq 0$, Lemma 2 holds trivially. Therefore, we focus on the remaining case where $q(\theta^*)$ 0, which means the constraint is violated and Eq. (14) and Eq.(15) simplifies to

$$g(\boldsymbol{\theta^*}) = \beta \lambda^*, \tag{16}$$

$$-\frac{\partial f}{\partial \theta}\Big|_{\theta=\theta^*} + \lambda^* \frac{\partial g}{\partial \theta}\Big|_{\theta=\theta^*} = \mathbf{0}$$
Substituting Eq.(16) into Eq.(17), we obtain

$$-\frac{\partial f}{\partial \boldsymbol{\theta}}|_{\boldsymbol{\theta}=\boldsymbol{\theta}^*} + \frac{g(\boldsymbol{\theta}^*)}{\beta} \frac{\partial g}{\partial \boldsymbol{\theta}}|_{\boldsymbol{\theta}=\boldsymbol{\theta}^*} = 0.$$
 (18)

We note that $g(\theta^*)$ is a scalar, meaning that each elements of $\frac{\partial f}{\partial \theta}|_{\theta=\theta^*}$ is proportional to the corresponding elements in $\frac{\partial g}{\partial \theta}|_{\theta=\theta^*}$ by the same constant $\frac{g(\theta^*)}{\beta}>0$. This allows us to pick any element of θ to analyze $g(\theta^*)$. (Note that when $\hat{\theta} \in \mathbb{R}^d$ is high-dimensional, Eq.(18) is challenging to achieve, because we need one scalar to satisfy all d equations. In practice, we observe small oscillations when the algorithm converges, which implies the algorithm finds it hard to exactly satisfy all equations.)

Denote $\phi_i = \phi(\boldsymbol{x_i}, a_i, y_i)$, $\Delta_i = \frac{\partial S(\boldsymbol{x_i}; \boldsymbol{\theta})}{\partial \theta_j} \Big|_{\boldsymbol{\theta} = \boldsymbol{\theta}^*} \leq L$, $\mu_{\Delta} = \mathbb{E}\Delta_i$, where $j = \arg\max_{\boldsymbol{\lambda}} \frac{\mu_{\Delta}}{L}$. The definition of function f (Eq.(3)) results in

$$\begin{split} \left| \frac{\partial f}{\partial \theta_{j}} \right|_{\boldsymbol{\theta} = \boldsymbol{\theta}^{\star}} &= \left| \frac{\sum_{i=1}^{n} \phi_{i} \Delta_{i} \sum_{s=1}^{n} S(\boldsymbol{x}_{s}; \boldsymbol{\theta})}{\left(\sum_{i=1}^{n} S(\boldsymbol{x}_{i}; \boldsymbol{\theta})\right)^{2}} - \right. \\ &\left. \frac{\sum_{i=1}^{n} \Delta_{i} \sum_{s=1}^{n} \phi_{s} S(\boldsymbol{x}_{s}; \boldsymbol{\theta})}{\left(\sum_{i=1}^{n} S(\boldsymbol{x}_{i}; \boldsymbol{\theta})\right)^{2}} \right| \\ &= \left| \frac{\sum_{i=1}^{n} \sum_{s=1}^{n} \Delta_{i} S(\boldsymbol{x}_{s}; \boldsymbol{\theta}) (\phi_{i} - \phi_{s})}{\left(\sum_{i=1}^{n} S(\boldsymbol{x}_{i}; \boldsymbol{\theta})\right)^{2}} \right| \end{split}$$

With $\phi_{max} = \max_i |\hat{\phi}(x_i, a_i, y_i)|$, we have,

$$\left| \frac{\partial f}{\partial \theta_{j}} \right|_{\boldsymbol{\theta} = \boldsymbol{\theta}^{*}} \le 2\phi_{max} \left| \frac{\sum_{i=1}^{n} \sum_{s=1}^{n} \Delta_{i} S(\boldsymbol{x}_{s}; \boldsymbol{\theta})}{\left(\sum_{i=1}^{n} S(\boldsymbol{x}_{i}; \boldsymbol{\theta})\right)^{2}} \right|
= 2\phi_{max} \left| \frac{\sum_{i=1}^{n} \Delta_{i} \sum_{s=1}^{n} S(\boldsymbol{x}_{s}; \boldsymbol{\theta})}{\left(\sum_{i=1}^{n} S(\boldsymbol{x}_{i}; \boldsymbol{\theta})\right)^{2}} \right|
= 2\phi_{max} \frac{\left|\sum_{i=1}^{n} \Delta_{i}\right|}{\sum_{i=1}^{n} S(\boldsymbol{x}_{i}; \boldsymbol{\theta})}$$
(19)

Substituting Eq. (19) into Eq. (18) and take assoluate value,

$$g(\boldsymbol{\theta}^*) \le \beta \left(\left| \frac{\partial g}{\partial \boldsymbol{\theta}} |_{\boldsymbol{\theta} = \boldsymbol{\theta}^*} \right| \right)^{-1} \frac{2\phi_{max} \left| \sum_{i=1}^n \Delta_i \right|}{\sum_{i=1}^n S(\boldsymbol{x}_i; \boldsymbol{\theta})}$$
(20)

Next, we will prove the upper bound of the group size constraint violation and the general linear constraints violation by analyzing $\frac{\partial g}{\partial \theta}|_{\theta=\theta^*}$.

Case 1: $g(\theta^*) = c - \frac{1}{n} \sum_{i=1}^n S(x_i; \theta^*) > 0$: the group size constraint is violated.

$$\frac{\partial g}{\partial \theta_j}|_{\boldsymbol{\theta} = \boldsymbol{\theta}^*} = -\frac{1}{n} \sum_{i=1}^n \Delta_i$$

Substituting this into Eq. (20):

$$g(\boldsymbol{\theta}^*) \leq \beta \left(\left| -\frac{1}{n} \sum_{i=1}^n \Delta_i \right| \right)^{-1} \frac{2\phi_{max} \left| \sum_{i=1}^n \Delta_i \right|}{\sum_{i=1}^n S(\boldsymbol{x_i}; \boldsymbol{\theta})}$$
$$= \beta \frac{2\phi_{max}}{\frac{1}{n} \sum_{i=1}^n S(\boldsymbol{x_i}; \boldsymbol{\theta})}$$
(21)

Substitute $\beta \leq \frac{\xi(c-\xi)\mu_{\Delta}}{2\phi_{max}L}$ into Eq. (21), we obtain

$$g(\boldsymbol{\theta^*}) \le \frac{\xi(c-\xi)\mu_{\Delta}}{\frac{1}{n}\sum_{i=1}^{n}S(\boldsymbol{x_i};\boldsymbol{\theta})L} \le \frac{\xi(c-\xi)}{\frac{1}{n}\sum_{i=1}^{n}S(\boldsymbol{x_i};\boldsymbol{\theta})} = \frac{\xi(c-\xi)}{c-g(\boldsymbol{\theta^*})}$$

Solving for $g(\theta^*)$, we obtain $g(\theta^*) \leq \xi$ (group size constraint satisfied) or $g(\theta^*) \geq c - \xi$ (the model collapses, group size is near zero).

Next, we show that the model is improbable to collapse if the feasible region is non-negligible.

Define the collapsed region as

$$\mathbf{\Theta}_{ ext{collapse}} := \left\{ oldsymbol{ heta} \in \Theta : rac{1}{n} \sum_{i=1}^{n} S(oldsymbol{x}_i; oldsymbol{ heta}) < \xi
ight\},$$

and the feasible region as

$$oldsymbol{\Theta}_{ ext{feasible}} := \Big\{ oldsymbol{ heta} \in \Theta : rac{1}{n} \sum_{i=1}^n S(oldsymbol{x}_i; oldsymbol{ heta}) \geq c$$

and other constraints are met \

for some thresholds $0 < \xi \ll c < 1$. Suppose that the volume of the feasible region dominates that of the collapsed region, i.e.,

$$|\Theta_{\text{collapse}}| \ll |\Theta_{\text{feasible}}|$$
.

Given $\forall i, 0 \leq S(x_i; \theta) \leq 1$, using Hoeffding inequality, we obtain

$$P\left(\sum_{i=1}^n S(\boldsymbol{x_i};\boldsymbol{\theta}) - \mathbb{E}\sum_{i=1}^n S(\boldsymbol{x_i};\boldsymbol{\theta}) \le -t\right) \le \exp(-\frac{2t^2}{n}).$$

Let $t = \sqrt{\frac{n \log(1/\delta)}{2}}$, with probability at least $1 - \delta$, we have

$$\sum_{i=1}^{n} S(\boldsymbol{x_i}; \boldsymbol{\theta}) - \mathbb{E} \sum_{i=1}^{n} S(\boldsymbol{x_i}; \boldsymbol{\theta}) \geq -\sqrt{\frac{n \log(1/\delta)}{2}}$$

Assume θ is sampled uniformly from $\Theta_{\text{collapase}} \cup \Theta_{\text{feasible}}$, $|\Theta_{collapase}| \ll |\Theta_{feasible}| \Rightarrow P(\theta \in \Theta_{\text{collapse}}) \ll P(\theta \in \Theta_{\text{collapase}})$

 Θ_{feasible}). Then,

$$\begin{split} \mathbb{E} \sum_{i=1}^{n} S(\boldsymbol{x_i}; \boldsymbol{\theta}) &= P(\boldsymbol{\theta} \in \Theta_{collapse}) \cdot \sum_{i=1}^{n} S(\boldsymbol{x_i}; \boldsymbol{\theta}) \\ &+ P(\boldsymbol{\theta} \in \Theta_{feasible}) \cdot \sum_{i=1}^{n} S(\boldsymbol{x_i}; \boldsymbol{\theta}) \end{split}$$

Given that the contribution from $\Theta_{collapse}$ is negligible, we approximate:

$$\mathbb{E}\sum_{i=1}^{n} S(\boldsymbol{x_i}; \boldsymbol{\theta}) \approx \sum_{i=1}^{n} S(\boldsymbol{x_i}; \boldsymbol{\theta}) | \{ \boldsymbol{\theta} \in \Theta_{feasible} \} \ge nc$$

Therefore, with probability at least $1 - \delta$, we have

$$\sum_{i=1}^{n} S(\boldsymbol{x_i}; \boldsymbol{\theta}) \ge \mathbb{E} \sum_{i=1}^{n} S(\boldsymbol{x_i}; \boldsymbol{\theta}) - \sqrt{\frac{n \log(1/\delta)}{2}}$$
$$\ge nc - \sqrt{\frac{n \log(1/\delta)}{2}}$$
$$\implies \frac{1}{n} \sum_{i=1}^{n} S(\boldsymbol{x_i}; \boldsymbol{\theta}) \ge c - \sqrt{\frac{\log(1/\delta)}{2n}},$$

i.e. the model is improbable to collapse if the feasible region is non-negligible.

Case 2: $g(\theta^*) = a^k + b^{k\top} S(x; \theta) > 0$: Similarly, we have

$$g(\boldsymbol{\theta}^*) \le \beta \left(\left| \sum_{i=1}^n b_i^k \Delta_i \right| \right)^{-1} \frac{2\phi_{max} \left| \sum_{i=1}^n \Delta_i \right|}{\sum_{i=1}^n S(\boldsymbol{x_i}; \boldsymbol{\theta})}. \tag{22}$$

Let $Z=\sum_{i=1}^n b_i^k \Delta_i$, then $\mathbb{E} Z=\sum_{i=1}^n b_i^k \mathbb{E} \Delta_i=\mu_{\Delta}\sum_{i=1}^n b_i^k$

By the triangle inequality, we have $\Big||Z|-|\mathbb{E}Z|\Big| \leq |Z-\mathbb{E}Z|$. So, by the Hoeffding inequality, we obtain

$$\begin{split} P(\left||Z| - |\mathbb{E}Z|\right| &\geq t) \leq P(|Z - \mathbb{E}Z| \geq t) \\ &\leq 2\exp(-\frac{2t^2}{4L^2\sum_{i=1}^n (b_i^k)^2}) \end{split}$$

Let $t = L\sqrt{2\sum_{i=1}^n (b_i^k)^2\log\frac{2}{\delta}}$. Then with probability at least $1-\delta$,

$$|Z| \ge |\mathbb{E}Z| + t = |\mu_{\Delta} \sum_{i=1}^{n} b_i^k| + t.$$

Substituting this into Eq. (22), we obtain

$$g(\boldsymbol{\theta^*}) \leq \beta \frac{2\phi_{max} \left| \sum_{i=1}^{n} \Delta_i \right|}{\left(\left| \mu_{\Delta} \sum_{i=1}^{n} b_i^k \right| + t \right) \sum_{i=1}^{n} S(\boldsymbol{x_i}; \boldsymbol{\theta})}$$

$$\leq \beta \frac{2\phi_{max} \sum_{i=1}^{n} \left| \Delta_i \right|}{\left(\left| \mu_{\Delta} \sum_{i=1}^{n} b_i^k \right| + t \right) \sum_{i=1}^{n} S(\boldsymbol{x_i}; \boldsymbol{\theta})}$$

$$\leq \beta \frac{2\phi_{max} L}{\left(\left| \mu_{\Delta} \sum_{i=1}^{n} b_i^k \right| + t \right) \frac{1}{n} \sum_{i=1}^{n} S(\boldsymbol{x_i}; \boldsymbol{\theta})}$$

As analyzed in **Case 1**, when the feasible region is non-negligible, $\frac{1}{n}\sum_{i=1}^n S(\boldsymbol{x_i};\boldsymbol{\theta}) > c - \xi$ with high probability. Therefore.

$$\begin{split} g(\boldsymbol{\theta^*}) &\leq \beta \frac{2\phi_{max}L}{\left(|\mu_{\Delta}\sum_{i=1}^n b_i^k| + t\right)(c - \xi)} \\ &\text{Plug in } \beta \leq \frac{\xi(c - \xi)|\mu_{\Delta}|}{2\phi_{max}L}, \\ &\leq \frac{\xi|\mu_{\Delta}|}{|\mu_{\Delta}\sum_{i=1}^n b_i^k| + t} \\ &\leq \frac{\xi|\mu_{\Delta}|}{|\mu_{\Delta}\sum_{i=1}^n b_i^k| + L\sqrt{2\sum_{i=1}^n (b_i^k)^2\log\frac{2}{\delta}}} \\ &\leq \frac{\xi}{|\sum_{i=1}^n b_i^k| + \frac{L}{|\mu_{\Delta}|}\sqrt{2\sum_{i=1}^n (b_i^k)^2\log\frac{2}{\delta}}} \end{split}$$

By Cauchy-Schawarz inequality, we have $\sqrt{\sum_{i=1}^n (b_i^k)^2} \ge \frac{|\sum_{i=1}^n b_i^k|}{\sqrt{n}}$, therefore,

$$g(\boldsymbol{\theta^*}) \le \frac{\xi}{\left|\sum_{i=1}^n b_i^k\right| + \frac{L}{|\mu_{\Delta}|} \frac{\left|\sum_{i=1}^n b_i^k\right|}{\sqrt{n}} \sqrt{2\log\frac{2}{\delta}}}$$
$$= \frac{\xi}{\left|\sum_{i=1}^n b_i^k\right| \left(1 + \frac{L}{|\mu_{\Delta}|\sqrt{n}} \sqrt{\log\frac{2}{\delta}}\right)}$$

Put together Case 1 and Case 2, we finish the proof.

C Implementation Details

C.1 Selection of $\hat{\phi}$

 $\frac{\sum_{i=1}^{n} S(\boldsymbol{x}_i; \boldsymbol{\theta}) \hat{\phi}(\boldsymbol{x}_i, a_i, y_i)}{\sum_{i=1}^{n} S(\boldsymbol{x}_i; \boldsymbol{\theta})}$ can be used to represent the ATE estimated by different methods. And the following $\hat{\phi}_{iptw}$ and $\hat{\phi}_{aiptw}$, correspond to the ATE estimated using IPTW and AIPTW, respectively. *inverse probability of treatment weighting* (IPTW) and *augmented inverse probability of treatment weighting* (AIPTW), respectively. To clarify, $\phi(\boldsymbol{x}_i, a_i, y_i)$ does not depend on the parameter $\boldsymbol{\theta}$, these estimates are separated from the parametric surrogate model S.

$$\begin{split} \hat{\phi}_{\mathrm{iptw}}(\boldsymbol{x}_i, a_i, y_i) = & \frac{a_i}{\hat{e}(\boldsymbol{x}_i)} y_i - \frac{1 - a_i}{1 - \hat{e}(\boldsymbol{x}_i)} y_i, \\ \hat{\phi}_{\mathrm{aiptw}}(\boldsymbol{x}_i, a_i, y_i) = & \hat{\mu}_1(\boldsymbol{x}_i) - \hat{\mu}_0(\boldsymbol{x}_i) + \frac{a_i}{\hat{e}(\boldsymbol{x}_i)} (y_i - \hat{\mu}_1(\boldsymbol{x}_i)) \\ & - \frac{1 - a_i}{1 - \hat{e}(\boldsymbol{x}_i)} (y_i - \hat{\mu}_0(\boldsymbol{x}_i)). \end{split}$$

C.2 Synthetic Data Generation

Let $\sigma_X, \sigma_Y, \rho \in \mathbb{R}$ be fixed constants, and let $\beta_1, \beta_\tau, \omega \in \mathbb{R}^p$. Draw X according to a multi-variate normal distribu-

Dataset	Dragonnet	LR
Synthetic	0.10	0.10
MIMIC-IV	2.32	1.57
eICU	1.08	1.10

Table C.3: Number of unbalance features after reweighting by propensity scores obtained by propensity models

tion, and A, Y(0), Y(1) as follows:

$$\boldsymbol{X} \sim \mathcal{MVN}(0, \sigma_X^2[(1-\rho)I_p + \rho 1_p 1_p^T]), \tag{23}$$

$$A|\mathbf{X} \sim \text{Bernoulli}(\sigma(\mathbf{X}^T \omega)),$$
 (24)

$$\epsilon \sim \mathcal{N}(0, \sigma_V^2),$$
 (25)

$$Y(0) = (\sin(10 * \mathbf{X}) + 5 * \mathbf{X}^{2})^{T} \beta_{1} + \epsilon,$$
(26)

$$Y(1) = (\sin(10 * \mathbf{X}) + 5 * \mathbf{X}^{2})^{T} \beta_{1} + \mathbf{X}^{T} \beta_{\tau} + \epsilon.$$
 (27)

We set the parameters as follows:

$$\begin{split} p &= 10, \quad \sigma_X = \sigma_Y = 0.1, \quad \rho = 0.3, \\ \beta_1 &= [0, 0, 0, 0, 2, 0, 0, 0, 0, 0], \\ \beta_\tau &= [0.5, 0.5, 0.5, 0.5, 0, 0, 0, 0, 0, 0], \\ \omega &= [0, -1 \cdot \tilde{\omega}, -1 \cdot \tilde{\omega}, 1 \cdot \tilde{\omega}, -2 \cdot \tilde{\omega}, 0, 0, 0, 0]. \end{split}$$

The *imbalance parameter*, $\tilde{\omega} \geq 0$, scales the magnitude of the treatment assignment weight vector ω . In particular, we generated two synthetic datasets with (1) no confounding bias ($\tilde{\omega}=0$); and (2) high confounding bias ($\tilde{\omega}=5$). As there is no limitation to generate synthetic data, we set up the total sample size for synthetic data as 5,000 to study the model performance under finite samples and use a balance 50/50 train-test split ratio. As for real-world datasets, we use a 70/30 train-test split.

C.3 Baseline Implementation

CAPITAL identifies a subgroup by maximizing its size while ensuring the CATE exceeds a predefined threshold. Since subgroup size is not directly controlled in this setting, we vary the CATE threshold and construct the group size vs. ATE curve for comparison.

OWL is originally designed for individual treatment rule estimation but can be viewed as a subgroup identification method without interpretability constraints. It assigns scores between 0 and 1, which we threshold to obtain subgroups of a desired size. We implement OWL using the DTRlearn2 R package.

VT The original VT supports both binary and continuous outcomes, but the commonly used R package a Virtual Twins handles only binary outcomes. Since our experiments require both, we implemented our own VT following (Foster, Taylor, and Ruberg 2011): first estimating treatment effects with a random forest, and then fitting a regression tree to assign subgroup scores. Subgroups of different sizes are obtained by thresholding these scores.

Dragonnet & CT & CF We adopts the implementations from the Python package causalml.

C.4 Model Selection for Nuisance Function Estimation

We consider LR and Dragonnet for estimating the propensity score model. We following the literature (Zang et al. 2023) to use the number of unbalanced features after inverse propensity score weighing as the metric (the lower the better) to select the propensity score model. The results are shown in Table C.3, which shows that LR performs better or equivalently than Dragonnet. Thus we select LR as the propensity score model for all datasets.

For the potential outcome model, we consider Dragonnet, CF, and CT, as they are the CATE estimators we are comparing against in subgroup identification. Theoretically, CF improves upon CT by reducing bias and producing smoother decision boundaries through aggregating CTs. As for Dragonnet and CF, prior work (Kiriakidou and Diou 2022) has shown that Dragonnet outperforms CF.

While many other methods exist for nuisance function estimation, our goal is to demonstrate MOSIC's flexibility rather than prescribe a specific estimator. If more effective models are developed or if a particular method performs better in a given setting, we encourage adapting those for nuisance function estimation.

C.5 Hyperparameter Tuning

CAPITAL optimizes the policy tree depth with $max_depth \in \{2,3\}$. VT selects decision tree depth for subgroup identification from $max_depth \in \{3,5,7,10\}$. Similarly, CT uses $max_depth \in \{3,5,7,10\}$, while CF considers both tree depth $max_depth \in \{3,5,7,10\}$ and the number of trees $num_tree \in \{5,10,20,50,100\}$. Moreover, Dragonnet tunes the hidden layer size with $hidden_size \in \{50,100,200\}$. Finally, the hyperparameters for our method include $\beta \in \{10^{-2},10^{-3},10^{-4},10^{-5}\}$ and those depending on the implementation of the subgroup identification model. For MOSIC-MLP, we tune the hidden layer size with $hidden_size \in \{50,100,200\}$.

D Significance Tests on Read-world data

Tables D.4 and D.5 present the p-values comparing MOSIC ($\alpha=0.01$) against baseline methods, corresponding to the hypothesis test that MOSIC is different than the baselines. These results directly support the performance trends shown in Figure 2. For instance, in eICU experiments with c=0.5:

- MOSIC achieves significantly better ATE than Dragonnet (p=0.0057)
- MOSIC maintains significantly fewer unbalanced features than Dragonnet (p=9.2E-04)

		c = 0.4	c = 0.5	c = 0.6	c = 0.7	c = 0.8
	CT	0.71	0.065	0.0011	0.0046	0.025
	CF	0.19	0.0048	0.00019	0.0012	0.0057
ATE	CA*	-	-	-	3.5E-05	-
AIL	DR*	0.30	0.0057	5.5E-04	0.011	0.11
	OWL	0.27	0.0019	0.0010	0.084	0.16
	VT	0.38	0.07	0.039	0.31	0.46
	CT	0.16	0.58	0.56	0.65	0.04
Balance	CF	0.35	0.12	0.48	0.47	0.16
	CA*	-	-	-	0.59	-
	DR*	0.022	9.2E-04	0.14	0.33	0.066
	OWL	0.0088	0.0077	0.13	0.22	0.046
	VT	0.0011	0.0060	0.036	0.23	0.39

Table D.4: eICU: p-values for ATE and feature balance comparisons between MOSIC and baseline methods.CA*: CAP-ITAL; DR*: Dragonnet.

		c = 0.5	c = 0.6	c = 0.7	c = 0.8
	CT	-	-	-	0.02
	CF	0.42	0.68	0.35	0.16
ATE	CA*	0.021	-	0.30	0.72
AIL	DR*	0.039	0.10	0.21	0.30
	VT	0.10	0.16	0.15	0.15
	CT	-	-	-	0.63
	CF	0.19	5.1E-04	1.3E-04	1.1E-04
Balance	CA*	6.3E-07	-	0.17	3.3E-05
Darance	DR*	0.062	0.80	0.28	0.48
	VT	0.033	0.0020	0.018	0.20

Table D.5: MIMIC: p-values for ATE and feature balance comparisons between MOSIC and baseline methods. CA*: CAPITAL; DR*: Dragonnet.

E Additional Experiment Results

E.1 Subgruop Identification on Unconfounded Synthetic data($\tilde{\omega} = 0$)

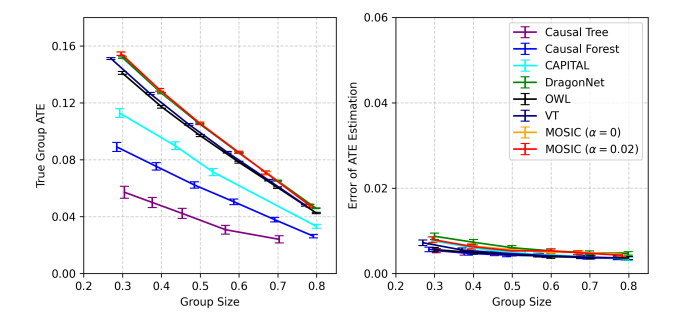


Figure E.1.1: True ATE and ATE estimation error across different group sizes on confounded synthetic data($\omega = 0$).

E.2 MOSIC with interpretability restriction

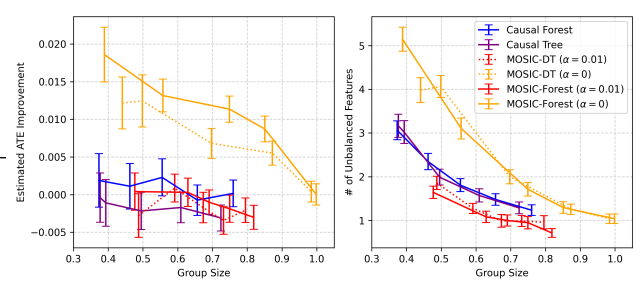


Figure E.2.1: Results on eICU. MOSIC-DT and CT use a single tree with depth = 5; MOSIC-Forest and CF use 3 trees with depth = 5. Mean \pm standard error across 100 random splits are reported.

E.3 Overlap constraint on synthetic data

We numerically verify that MOSIC can indeed accommodate the overlap constraint (Figure E.3.1). To assess its effect on estimation error, we conduct experiments on the confounded synthetic data with varying α values. Figure E.3.1(a) is generated by a random instance of the 100 random train-test splits presented in Figure E.3.1(b). In Figure E.3.1(a), each dot represents an individual, with the x-axis denoting the estimated propensity score, the y-axis representing the true individual treatment effect (ITE), and the vertical lines indicating the desired overlap threshold. Without overlap constraints, MOSIC selects patients with the highest ITEs.

With overlap constraints (Figure E.3.1(a), left), MOSIC continues to select patients with large ITEs but systematically excludes those who violate the overlap constraint $(\hat{e}(x) < 0.05 \text{ or } \hat{e}(x) > 0.95)$. Figure E.3.1(b) further quantifies the effect of excluding patients with limited overlap by reporting the estimation error and the number of unbalanced features.

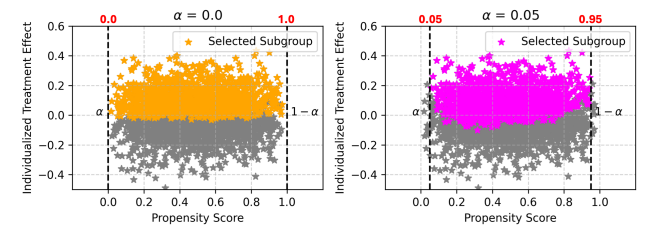
As the desired overlap threshold α increases, the estimation error of the subgroup ATE decreases, suggesting that enforcing stronger overlap improves estimation reliability. Meanwhile, stronger overlap also correlates with a lower number of unbalanced features.

E.4 Extension to Safety, Budget, and Fairness Constraint on Synthetic Data

To demonstrate MOSIC's flexibility to handle additional constraints, we extend the synthetic data generation process described in Appendix C.2 by introducing a safety, budget, and fairness constraint. In particular:

• Safety constraint: Following Doubleday et al. (2022), each sample is assigned a risk score $r_i = 1/(1+\exp(10*x_i[10]+1))$. We require the average risk of the selected subgroup to be no greater than 0.05:

$$\frac{\sum_{i=1}^{n} \mathbb{1}(S(x_i) > 0.5)r_i}{\sum_{i=1}^{n} \mathbb{1}(S(x_i) > 0.5)} \le 0.05.$$



(a) Characteristics of the Identified Samples

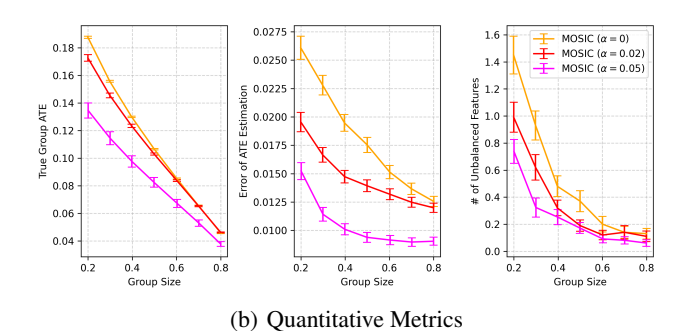


Figure E.3.1: Results on synthetic data with confounding bias ($\tilde{\omega} = 5$), obtained using MOSIC with varying α .

Budget constraint: Following Qiu, Carone, and Luedtke (2022), each sample is assigned a treatmentd cost value cost_i = (x_i[3] + 5)/5. The total cost of the selected subgroup must not exceed half the cost of treating the entire population (assuming a unit cost per sample):

$$\sum_{i=1}^{n} \mathbb{1}(S(x_i) > 0.5) cost_i \le 0.5 * n.$$

The test contains 2500 samples, so the total cost limit 0.5 * n = 1250 in this case.

• Fairness constraint: Let a binary sensitive attribute: $sens_i = \mathbb{1}(x[3] > 0.5)$. We adopt the conditional statistical parity metric (Mehrabi et al. 2021). In our setting, this corresponds to maintaining a sensitive-group proportion of 0.5 in the selected subgroup.:

$$\left| \frac{\sum_{i=1}^{n} \mathbb{1}(S(x_i) > 0.5)sens_i}{\sum_{i=1}^{n} \mathbb{1}(S(x_i) > 0.5)} - 0.5 \right| \le 0.01,$$

where we allow a violation of 0.01. We can then convert this to two ratio-form constraints:

$$-0.01 \le \frac{\sum_{i=1}^{n} \mathbb{1}(S(x_i) > 0.5)sens_i}{\sum_{i=1}^{n} \mathbb{1}(S(x_i) > 0.5)} - 0.5 \le 0.01.$$

In addition to the group size constraint (c=0.5) and overlap constraint($\alpha=0.02$), we progressively add the following constraints: 1) Plus safety constraint; 2) Plus safety and budget constraint; 3) Plus safety, budget, and fairness constraint. Results in Table E.4.1 show that MOSIC can effectively enforce all of these constraints.

E.5 Extension to Safety Constraint on eICU

The Glasgow Coma Scale (GCS), a core component of the Sequential Organ Failure Assessment (SOFA) score, measures level of consciousness, with lower scores indicating more severe dysfunction. We targeted patients with GCS < 6 because this threshold represents the most severe central nervous system dysfunction in the SOFA score, the most commonly-used ICU metric. Without a constraint on the GCS score, we observed that the selected subgroup contains a nontrivial number of patients with GCS < 6. As observational studies have shown that glucocorticoids may exacerbate neural system damage, such a subgroup raises a safety concern. Therefore, we required that the proportion of patients with GCS < 6 remain below 0.05. We did not enforce a strict exclusion (i.e., a threshold of 0) because it is possible that some patients with severe neural dysfunction could still derive meaningful benefit from the treatment.

To impose the interpretability requirement, we implement MOSIC-DT for this setting. Similarly, we run experiments on 100 random train-test splits and use 5-fold cross-validation to select the tree depth among {3,5,7}. Results in Table 2 show MOSIC can effectively exclude patients with GCS< 6. Additionally, an example (Figure E.5.1) shows that MOSIC indeed learned to exclude such high-risk patients.

F Evaluation on Binary Subgroup Setting

Unlike approaches that assume the existence of two or a finite number of subgroups with distinct ATEs, our study focuses on identifying a subset of the population with maximal ATE under real-world constraints, without making structural assumptions about the underlying heterogeneity. This design enables our method to generalize to continuous or complex heterogeneity. Nevertheless, we recognize that such structural assumptions, such as that binary subgroups with distinct ATE exist, are plausible in certain real-world scenarios. In such cases, the real-world constraint will naturally introduce a trade-off for identification performance.

To illustrate, we modify the DGP of synthetic data by replacing Y(1) in Appendix C.2 to:

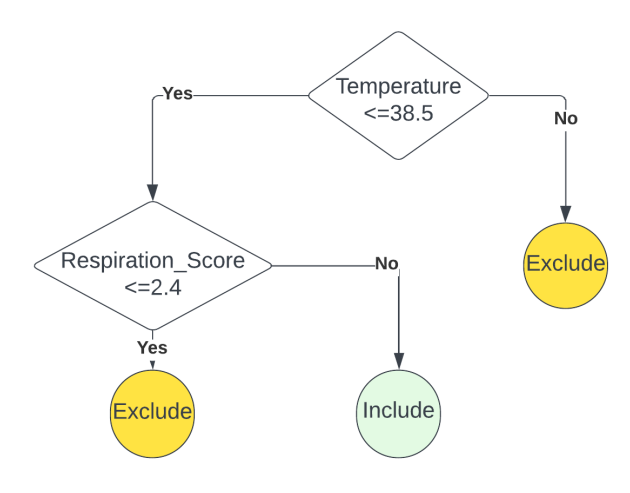
$$Y(1) = (\sin(10 * \mathbf{X}) + 5 * \mathbf{X}^{2})^{T} \beta_{1} + \mathbb{1}(\mathbf{X}^{T} > 0.05)\beta_{\tau} + \epsilon.$$

That says, only patients with covariates > 0.05 at positive β_{τ} indices receive a positive effect; others receive none. This yields a positive subgroup comprising 68% of samples. Using this DGP, we test MOSIC with beta = 1e-5, alpha = 0, and c in $\{0.6, 0.7, 0.8\}$. The precision and recall of subgroup identification are evaluated. Results in Table F.0.1 are reported as mean \pm standard deviation over 100 runs. Performance aligns with theory: precision/recall degrade when c (the group size constraint) exceeds/falls below the true subgroup size, reflecting constraint-driven trade-offs.

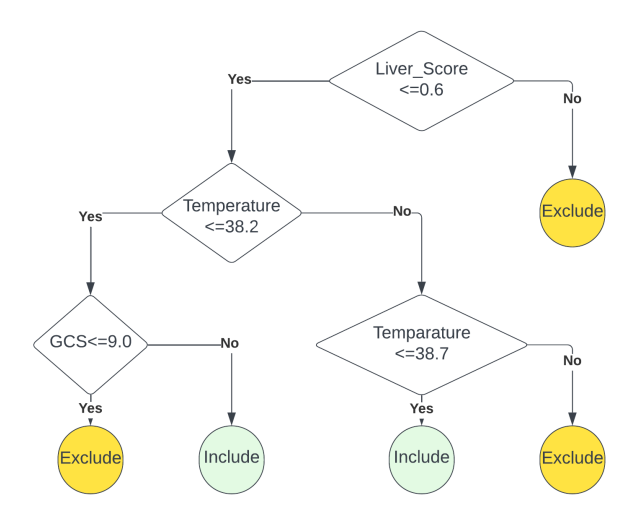
Table E.4.1: Performance on synthetic data ($\tilde{\omega} = 5$) under multiple additional constraints.

Metric	Group Size and Overlap	+Safety	+Safety+Budget	+Safety+Budget+Fairness
Group Size	0.50 ± 0.01	0.50 ± 0.05	0.48 ± 0.05	0.49 ± 0.02
# Unbalance	0.14 ± 0.40	0.20 ± 0.45	0.23 ± 0.57	0.23 ± 0.45
True CATE	0.10 ± 0.01	0.10 ± 0.01	0.09 ± 0.01	0.09 ± 0.01
ATE Error	0.01 ± 0.01	0.01 ± 0.01	0.01 ± 0.01	0.01 ± 0.01
Average Risk	0.08 ± 0.01	0.05 ± 0.01	0.05 ± 0.01	0.05 ± 0.01
Total Cost	1377.41 ± 41.57	1365.72 ± 144.95	1252.78 ± 132.59	1268.40 ± 42.44
Sensitive Group Ratio	0.45 ± 0.03	0.45 ± 0.03	0.46 ± 0.03	0.49 ± 0.02

^{*}Constraints: 1) Safety: Average Risk ≤ 0.05 ; 2) Budget: Total Cost ≤ 1250 ; 3) Fairness: |Sensitive Group Ratio - 0.5| ≤ 0.01 .



(a) Without GCS constraint



(b) With GCS constraint

Figure E.5.1: A returning DT from the same split on eICU with and without the GCS < 6 constraint.

c	ATE	Group Size	Precision	Recall
0.6	0.92 ± 0.07	0.60 ± 0.01	0.93 ± 0.05	0.83 ± 0.05
0.7	$0.84 {\pm} 0.05$	0.70 ± 0.01	0.88 ± 0.04	0.92 ± 0.04
0.8	0.75 ± 0.04	$0.80 {\pm} 0.01$	0.80 ± 0.03	0.96 ± 0.04

Table F.0.1: Performance of binary subgroup identification

G Evaluation of Type I error

Although our primary focus is on multi-constraint subgroup identification rather than statistical inference, we also evaluate Type I error of the identified subgroup. We use a data-splitting approach to test whether identified subgroups arise spuriously under the null hypothesis, where all individuals have zero treatment effect. Using data splitting, Type I error of the selected subgroup can be evaluated after we build the subgroup assignment model. Specifically:

- 1. Split the dataset (e.g., 50-50) into training (subgroup selection) and holdout (inference);
- 2. Train MOSIC on the training set to learn the subgroup model;
- 3. Apply the model to the holdout set to identify the subgroup, then compute its subgroup ATE, denoted as ATE_{hold_out}
- 4. Test the null hypothesis on the holdout set:
- (a) Construct the distribution of subgroup ATE under the null (here by directly sampling from the test distribution, with bootstrap subsample size equaling the target subgroup size specified by the parameter *c*)
- (b) Compare ATE_{hold_out} to this distribution, and determine whether the null hypothesis should be rejected.
- 5. Repeat steps 1-4 on additional synthetic data instances, aggregate results, and estimate type-I error.

We generated 100 synthetic datasets using the same DGP in Appendix C.2 except that β_{τ} is set to 0. This aligns with the null hypothesis: all individuals have zero treatment effect. For each instance, we set the bootstrap iterations to 10000. Type I error rate is computed as the proportion of instances in which the null hypothesis is rejected by 5% significance level.

As shown in Table G.0.1, the Type I error rate increases when the parameter c is small, consistent with theoretical expectations. Smaller subgroups lead to higher variance in ATE estimates, highlighting a fundamental trade-off between real-world constraints and statistical reliability.

С	ATE	Group Size	Type I error
0.4	-0.0011 ± 0.0401	0.3991 ± 0.0141	0.12
0.6	-0.0018 ± 0.0298	0.6020 ± 0.0141	0.00
0.8	-0.0000 ± 0.0212	0.8038 ± 0.0121	0.00

Table G.0.1: Type I error under different constraints for group size.